coatings

MDPI

Article

Synthesis and Characterization of Cadmium Ion-Imprinted/Natural Sand Composite and Research on Its Adsorption Properties

Aray Murat, Shuaibing Gao, Lingling Wang, Linlin Chai, Shawket Abliz * and Abliz Yimit

Key Laboratory of Oil and Gas Fine Chemicals of Ministry of Education, School of Chemical Engineering, Xinjiang University, Urumqi 830017, China; aray9518@163.com (A.M.); gsb1215@163.com (S.G.); w18340357067@163.com (L.W.); 18129226592@163.com (L.C.); ablizy@sina.com (A.Y.)

* Correspondence: shawket_abliz@sina.com

Abstract: Cadmium is a common heavy metal that can cause serious harm to human health, even in trace amounts. Therefore, it is of great significance to develop environmentally friendly, inexpensive, and readily available adsorbent materials with high selectivity. By preparing ion-imprinted composites on the surface of a suitable carrier through surface imprinting, the number of effective adsorption sites can be increased, and target ions can be more quickly identified. In this study, we synthesized a cadmium ion-imprinted/natural sand composite material (NS/Cd-IIP) using natural sand as the carrier, Cd(II) as the template ion, and acrylamide as the functional monomer. A series of characterization techniques were employed to confirm the composite. Static and dynamic adsorption experiments were conducted to investigate various factors affecting its adsorption performance. The optimum adsorption pH was found to be 7, and the adsorption equilibrium time was determined to be 105 min. The imprinted composites exhibited a static adsorption saturation capacity of 33.84 $mg \cdot g^{-1}$, which was significantly higher than that of the non-imprinted composites. The adsorption behavior of composites followed Langmuir isotherm and quasi-second-order kinetic. Thermodynamic parameters indicated that the adsorption process of NS/Cd-IIP for Cd(II) was exothermic, entropic, and spontaneous. The selectivity of NS/Cd-IIP towards Cd(II) was significantly higher than that towards other ions. By optimizing the dynamic adsorption conditions, the maximum adsorption capacity of NS/Cd-IIP was determined to be 3.77 $mg \cdot g^{-1}$, and the adsorption behavior conformed to the Thomas model. NS/Cd-IIP was used as a solid-phase extractant for trace determination of Cd(II) in tap water, achieving a recovery rate exceeding 101%.

Keywords: cadmium ion; adsorption; natural sand; ion imprinted composite

Citation: Murat, A.; Gao, S.; Wang, L.; Chai, L.; Abliz, S.; Yimit, A. Synthesis and Characterization of Cadmium Ion-Imprinted/Natural Sand Composite and Research on Its Adsorption Properties. *Coatings* **2023**, *13*, 1288. https://doi.org/10.3390/coatings13071288

Academic Editor: Alexandru Enesca

Received: 3 June 2023
Revised: 18 July 2023
Accepted: 21 July 2023
Published: 23 July 2023

1. Introduction

With the growth of the global population and rapid development of industry and agriculture, human activities such as excessive chemical usage have introduced a variety of toxic pollutants that significantly harm the environment. Among these pollutants, heavy metals are one of the primary causes of environmental pollution. Cadmium ion is one of the highly toxic heavy metals, with natural sources including marine phosphate, weathering, and volcanic activities. Anthropogenic industrial activities such as mining, electroplating, and the production of phosphate fertilizers, plastics, and nickel–cadmium batteries have the potential to release Cd(II) into the environment in the form of pollutants [1–3]. Cd(II) has a long half-life and is resistant to degradation. It can migrate to the soil and subsequently enter the human body through water and food. It is then transported by red blood cells and albumins into the bloodstream. Finally, it accumulates in organs such as the kidney, liver, and intestine, blocking the activity of necessary enzymes and affecting the immune function of the cells. During the mid-20th century, an outbreak of "Itai Itai" disease in Japan was caused by persistent Cd(II) poisoning. Even trace amounts of Cd(II) present significant

hazards to human health [4,5]. Cd(II) has been demonstrated to induce various types of cancer, and international health organizations have established a safe intake level of 25 μg cadmium per kilogram of body weight [6]. Therefore, urgent measures must be taken to develop techniques for isolating and enriching cadmium from the environment. While various techniques can be used for trace determination of cadmium, direct determination in real samples is subject to strong matrix interference.

Ion imprinting polymers (IIPs), which have similar preparation technology and principles to molecular imprinting technology (MIPs), were first introduced through the successful synthesis of molecularly imprinted polymers in 1972. In 1976, Nishide et al. [7] demonstrated the first application of metal ions in imprinting technology by preparing a copper ion-imprinted polymer through cross-linked polymerization of poly(4-vinyl pyridine) and 1,4-dibromopropane. IIPs exhibit excellent adsorption properties and imprinted cavities, which can selectively recognize metal ions without interference from other elements. The preparation of IIPs typically involves the use of template ions, functional monomers, crosslinkers, initiators, and solvents that are specifically targeted toward the template ions [8]. Zhou et al. [9] used the bulk polymerization method to prepare a Ni^{2+}-imprinted polymer with methacrylic acid (MAA) as the functional monomer, diphenylcarbapan (DPC) as the ligand, and azobisisobutyronitrile (AIBN) as the initiator. The resulting polymer exhibited a maximum adsorption capacity of 83.6 $mg \cdot g^{-1}$ for Ni^{2+}. It demonstrated the high affinity and selectivity of the polymer towards Ni^{2+} ions.

Traditional ion-imprinting techniques may lead to some problems, including excessive embedding of imprinted ions, resulting in difficulties with elution, weak affinity between imprinted sites and target ions, and poor mass transfer effect [10]. These factors can impact the adsorption performance of materials. Surface ion imprinting involves the polymerization reaction occurring on the surface of a solid-phase support [11]. In this process, recognition sites are distributed on the outer layer or surface of the support. The large specific surface area increases the number of effective adsorption sites. In comparison to the traditional ion-imprinting synthesis method, surface ion imprinting provides a greater number of adsorption sites, enabling faster identification of target ions. This ultimately enhances adsorption efficiency and reduces the embedding phenomenon [12]. Lv et al. [13] used mesoporous silica MCM-41 as a carrier to prepare a Cu^{2+}-imprinted polymer through surface imprinting technology. The polymer was then used as an adsorbent for selective removal of Cu^{2+} from lake water, exhibiting a high adsorption capacity of 87.8 $mg \cdot g^{-1}$. Liu et al. [14] used acetic acid to modify chitosan, with Ni^{2+} as the template ion and epchlorohydrin as a cross-linking agent to prepare an imprinted polymer with selective adsorption performance for Ni^{2+} through surface imprinting technology. The maximum adsorption capacity reached 20 $mg \cdot g^{-1}$. Silica material is commonly used as a carrier in surface ion imprinting technology due to its abundant hydroxyl groups, which serve as ideal grafting sites [15]. Natural materials rich in silica, such as diatoms [16] and sand [17], possess the advantages of having abundant sources and low prices, while being environmentally friendly [18]. They can serve as good carriers for ion-imprinted polymers. Shen et al. [19] used diatomite as the raw material, with NaOH and $MnCl_2$ as compound modifiers to prepare an adsorbent. Then, they investigated its adsorption performance on Cd(II). The results showed that the active silane chain on the surface of diatomite was opened during the modification process. A large number of manganese hydroxyl sites were formed on its surface, and the adsorption rate of Cd(II) was increased to 98.6%, indicating that modified diatomite can be effectively used as an adsorbent to remove Cd(II) from wastewater. Ma et al. [16] synthesized a new type of Cd(II)-imprinting adsorbent using surface imprinting technology. They used environmentally friendly and cheap diatom as the carrier, 3-mercaptopropyl trimethoxysiane as the functional monomer, and Cd(II) as the template ion. After optimizing the adsorption conditions, the diatom-based imprinting polymer exhibited an adsorption capacity of 11.64 $mg \cdot g^{-1}$, while the diatom had a capacity of 1.37 $mg \cdot g^{-1}$. These results clearly demonstrate that the surface imprinting method

significantly improved the adsorption capacity of diatoms. However, there is a lack of documentation regarding adsorption materials employing sand as carriers.

This study aimed to achieve selective adsorption of Cd(II) in water using imprinted composite materials. This research expands the application of natural materials such as natural sand, which are rich in resources but have not been effectively used in adsorption. Additionally, it provides a new strategy for addressing the compatibility issues between organic polymers and inorganic natural materials. Natural sand was silylated with γ-aminopropyltriethoxysilane and used as a carrier for the preparation of cadmium ion-imprinted composite materials. The template ions were cadmium ions, the functional monomer was acrylamide (AM), the cross-linking agent was ethylene glycol dimethacrylate (EGDMA), and potassium persulfate served as an initiator. Acrylamide, a functional monomer, was effectively incorporated onto the surface of silylated sand to create an inorganic carrier–organic functional group structure, using surface ion-imprinting technology to synthesize an ion-imprinted composite material with adsorption selectivity for Cd(II).

2. Materials and Methods

2.1. Experimental Reagents

Natural sand was collected from different points in the Taklimakan Desert (Xinjiang, China). γ-aminopropyltriethoxysilane (KH-550) was purchased from Sahn Chemical Technology Shanghai Co., Ltd. (Shanghai, China). Cadmium carbonate ($CdCO_3$) was purchased from Tianjin Damao Chemical Reagent Factory (Tianjin, China). Acrylamide (AM) was purchased from Tianjin Yongsheng Fine Chemical Co., Ltd. (Tianjin, China). Ethylene glycol dimethacrylate (EGDMA) was purchased from TCI Huacheng Industrial Development Co., Ltd. (Shanghai, China). Potassium persulfate (KPS) was purchased from Tianjin Zhiyuan Chemical Reagent Co., Ltd. (Tianjin, China). Sodium hydroxide (NaOH) was purchased from Tianjin Xinbote Chemical Co., Ltd. (Tianjin, China). Hydrochloric acid (HCl), Sulfuric acid (H_2SO_4), and Nitric acid (HNO_3) were purchased from Urumqi Dicheng Chemical Co., Ltd. (Urumqi, China). All reagents were analytically pure. All the solutions used were prepared with deionized water.

2.2. Experimental Instruments

The UV–vis spectra were recorded with an ultraviolet absorption spectrometer (T6, New Century, Dalian, China). The concentrations of ions were measured using an atomic absorption spectrometer (AA6800, Shimadzu, Kyoto, Japan). The infrared spectra were obtained by using a Fourier transform infrared spectrometer (FTIR) (EQUINOX55, Bruker, Saarbrucken, Germany). The surface morphology and energy dispersive X-ray spectroscopy (EDS) was obtained using an electron scanning electron microscope (SEM) (SU8010, Hitachi, Tokyo, Japan). X-ray photoelectron spectroscopy was obtained by using an X-ray photoelectron spectrometer (XPS) (ESCALAB 250 Xi, Thermo Fisher Scientific, Waltham, MA, USA).

2.3. Synthesis of Cd(II) Imprinted/Natural Sand Composite Material

2.3.1. Preparation of Cd(II)-AM Complex

Weighed 0.50 g of $CdCO_3$ in a beaker, dissolved it with 1–2 mL of 3 mol·L^{-1} hydrochloric acid, and added 50 mL deionized water. Then, the solution was transferred to a 100 mL round-bottom flask, and 0.82 g of AM was added. The mixture was stirred at 30–40 °C for 1 h to facilitate the coordination of Cd(II) with AM, resulting in the formation of a Cd(II)-AM solution. Then, the absorbance of the solution was measured with an ultraviolet spectrophotometer.

2.3.2. Preparation of NS/Cd-IIP and NS/Cd-NIP

Weighed 5 g of sand, and sieved the sand to a particle size of 0.076 mm. The sand was repeatedly washed with deionized water until the water became clear, then filtered and dried at 80 °C for 6 h. A 10 mL aqueous solution of KH-550 was prepared with a

ratio of 1:10. The sand was soaked in the solution for 16 h to generate silylated sand. The silylated sand, the synthetic Cd(II)–AM solution mentioned above, and 10.9 mL of cross-linking agent EGDMA were added to a 3-mouth round bottom flask with a stirrer and a thermometer. The reaction system was stirred under nitrogen protection. When the temperature was raised to 70 °C, 0.02 g of initiator KPS was added, and the reaction was continued under a nitrogen atmosphere for 7 h, resulting in the formation of polymer composites. The obtained polymer composites were washed several times with deionized water, filtered, and dried at 60 °C. Then, the polymer composite was repeatedly washed with 1 mol·L^{-1} HCl until the Cd(II) signal could no longer be detected with flame atomic absorption spectroscopy (FAAS). The non-imprinted polymer composite (NS/Cd-NIP) was prepared following the same method as above, except that Cd(II) was not added during synthesis. The preparation process is shown in Figure 1.

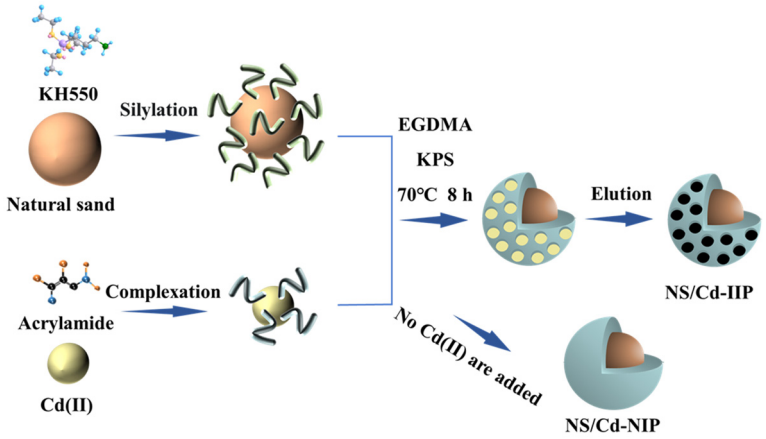

Figure 1. Preparation flow chart of natural sand/cadmium ion-imprinted composites.

2.4. Adsorption Experiments

2.4.1. Static Adsorption Experiment

The Cd(II) solution was added to a sealed centrifuge tube, and the pH value was adjusted accordingly. Subsequently, the NS/Cd-IIP, as an adsorbent, was added to the solution and allowed to reach adsorption equilibrium. The adsorption capacity, rate, and desorption rate were calculated according to Equations (1)–(3) [20]:

$$Q = \frac{(C_0 - C_e)V}{W} \quad (1)$$

$$E = \frac{C_0 - C_e}{C_0} \times 100\% \quad (2)$$

$$B = \frac{C_d V_d}{(C_0 - C_e)V} \times 100\% \quad (3)$$

where C_0 (mg·L^{-1}) and C_e (mg·L^{-1}) are initial concentration and adsorption equilibrium concentration of Cd(II) solution, respectively. C_d (mg·L^{-1}) is the desorption concentration of Cd(II) solution, V (L) is the volume of Cd(II) solution, V_d (L) is the volume of desorption solution, and W (g) is the weight of dry adsorbate.

2.4.2. Dynamic Adsorption Experiment

A certain amount of NS/Cd-IIP, as the adsorbent, was added into a microcolumn with an inner diameter of 5 mm. The flow rate for dynamic adsorption experiments was controlled with a peristaltic pump. The Cd(II) solution was passed through the microcolumn at a certain flow rate, and the Cd(II) solution flowing out of the column was quantitatively collected every 5 min. The concentration of Cd(II) in the solution was determined using

FAAS, and the dynamic adsorption penetration curve was drawn. After adsorption equilibrium, the adsorbent was washed with an acid solution, and the desorption solution was quantitatively collected. The desorption parameters were optimized by investigating the elution conditions. In order to explore the influence of different factors on dynamic adsorption, we conducted experiments by varying the filling height of the microcolumn, initial solution concentration, and loading flow rate. The dynamic adsorption capacity was calculated according to Equations (4)–(6) [21]:

$$q_e = \int_0^{V_e} (C_0 - C_t) dV/m \tag{4}$$

$$V_e = vt_e \tag{5}$$

$$q_{total} = q_e m \tag{6}$$

where q_e ($mg \cdot g^{-1}$) is the adsorption capacity of Cd(II), C_0 ($mg \cdot L^{-1}$) is the initial solution concentration, C_t ($mg \cdot L^{-1}$) is the outflow solution concentration at time t, m (g) is the adsorbent weight in the column, and v ($mL \cdot min^{-1}$) is the flow rate. q_{total} represents the total adsorption capacity of Cd(II) in the column. The breakthrough point was reached when C_t/C_0 = 10%, and the equilibrium point was achieved at C_t/C_0 = 90%. V_e (L) denotes the volume of solution that passed through the microcolumn at adsorption equilibrium.

The experimental data were fitted with a theoretical model to further describe the adsorption behavior. Due to the unstable state of the adsorption process when the solution flows through the column, it is difficult to express its dynamic behavior. Therefore, the Thomas and Adams–Bohart models were used here to predict the dynamic adsorption behavior of the breakthrough curve [22]. The equation of the Thomas model is as follows:

$$\frac{C_t}{C_0} = \frac{1}{1 + \exp\left(\frac{K_{Th} q_e m}{v} - K_{Th} C_0 t\right)} \tag{7}$$

where K_{Th} ($mL \cdot min^{-1} mg^{-1}$) is the Thomas constant.

The equation of the Adams–Bohart model is as follows:

$$\frac{C_t}{C_0} = \exp\left(C_0 t - K_A N_0 \frac{Z}{F}\right) \tag{8}$$

where K_A ($mL \cdot min^{-1} mg^{-1}$) is the rate constant of the Adams–Bohart, N_0 ($mg \cdot L^{-1}$) is the saturation concentration, Z (cm) is the height of the adsorbent in the column, and F ($cm \cdot min^{-1}$) is the flow rate of the loading line.

2.4.3. Selectivity Adsorption

To evaluate the selectivity of NS/Cd-IIP for Cd(II), competitive ions with the same charge and similar radius to Cd(II) were selected, including Cu(II), Mn(II), Ni(II), and Pb(II). The various parameters of the selectivity experiment were calculated according to Equations (9)–(11):

$$D = \frac{(C_0 - C_e)V}{C_e W} \tag{9}$$

$$\alpha = \frac{D_{Cd(II)}}{D_{M(II)}} \tag{10}$$

$$k = \frac{\alpha_{NS/Cd-IIP}}{\alpha_{NS/Cd-NIP}} \tag{11}$$

where D is the partition coefficient, M(II) is the competing ion, α is the selection coefficient, and k is the coefficient of relative selection.

2.4.4. Regeneration of NS/Cd-IIP

In practical applications, the regeneration performance of an adsorbent is a crucial parameter for its reuse. The saturated NS/Cd-IIP was used for adsorption–desorption experiments under optimized experimental conditions, and the Cd(II) content in the solution before and after adsorption was measured to evaluate the reuse performance of NS/Cd-IIP.

2.4.5. Actual Water Sample Analysis

The method of enrichment and separation by NS/Cd-IIP was applied for the detection of Cd(II) in real water samples, which were taken from tap water. The standard addition method was used to detect Cd(II) in water samples and the recovery rate of NS/Cd-IIP for Cd(II). The concentration of Cd(II) standard solution was 0, 5, and 10 $\mu g \cdot L^{-1}$.

3. Result and Discussion

3.1. Characterization Studies

3.1.1. SEM and EDS Analysis

The surface morphologies of NS/Cd-IIP were characterized before and after Cd(II) elution. Figure 2a,b show the morphologies of NS/Cd-IIP before elution, while Figure 2c,d depict the morphologies after elution. The imprinted composites exhibit a rough, heterogeneous, and porous surface that facilitated metal ion adsorption. The surface morphology changes before and after the elution of template ions. Before the elution, the imprinted composite's surface is relatively compact, while after elution, it becomes rougher with a more abundant and complex pore structure that enhances the specific surface area and adsorption sites for Cd(II), thereby improving adsorption capacity.

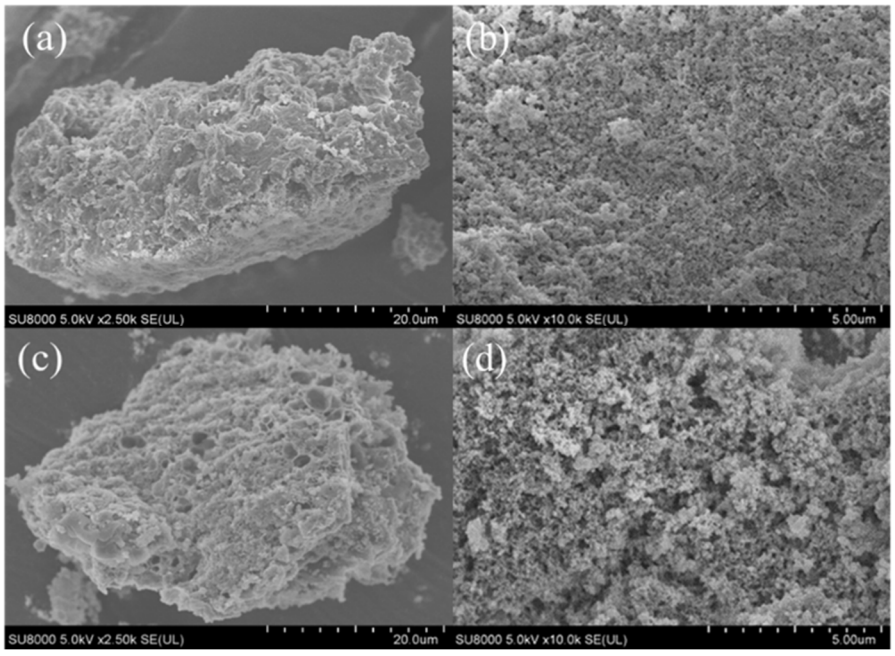

Figure 2. SEM images of NS/Cd-IIP: (**a**,**b**) before elution; (**c**,**d**) after elution.

The elemental composition of the NS/Cd-IIP surface was analyzed using EDS before and after the elution of template ions, as illustrated in Figure 3. Before the elution, the surface contained C, N, O, Si, and Cd. After elution, only C, N, O, and Si were detected with no trace of Cd(II), indicating the successful removal of template ions.

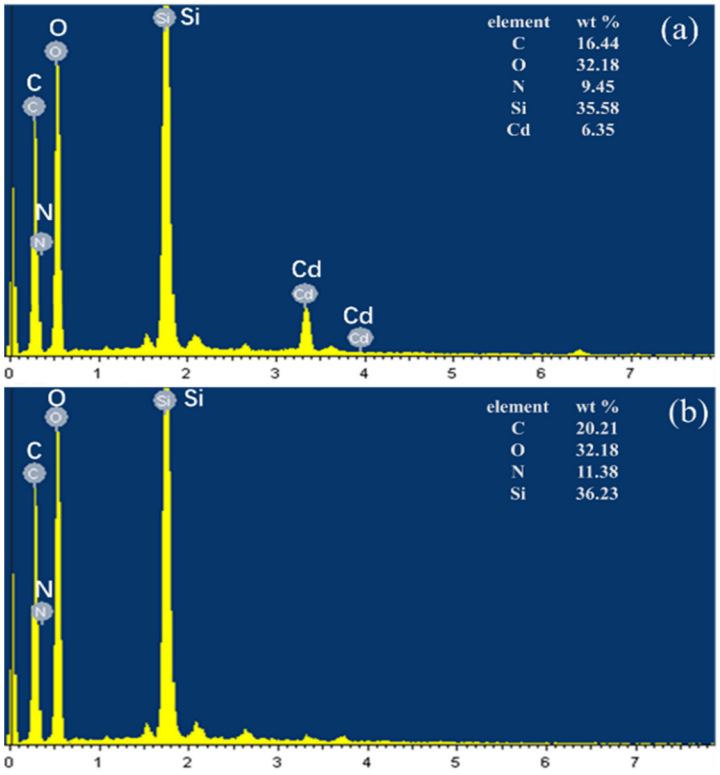

Figure 3. EDS images of NS/Cd-IIP before and after elution: (**a**) before elution; (**b**) after elution.

3.1.2. N_2 Adsorption–Desorption Analysis

The N_2 adsorption–desorption isotherms of NS/Cd-IIP and NS/Cd-NIP are shown in Figure 4, and the specific surface area and pore structure parameters are shown in Table 1. The typical type IV isotherms in the figure further confirm the mesoporous structure of NS/Cd-IIP. The specific surface areas of NS/Cd-IIP and NS/Cd-NIP are 65.19 $m^2 \cdot g^{-1}$ and 50.25 $m^2 \cdot g^{-1}$, respectively. The specific surface area of the non-imprinted composite was smaller than that of the imprinted composite because Cd(II) occupied a certain position during the imprinting process. After elution of Cd(II), some small cavities form on the surface of NS/Cd-IIP, effectively increasing the specific surface area. The above results indicate that the imprinted composite is a mesoporous material with a high specific surface area. The sand-based imprinted composite facilitates the exposure of adsorption sites and enhances the adsorption of template ions, thereby effectively increasing its adsorption capacity.

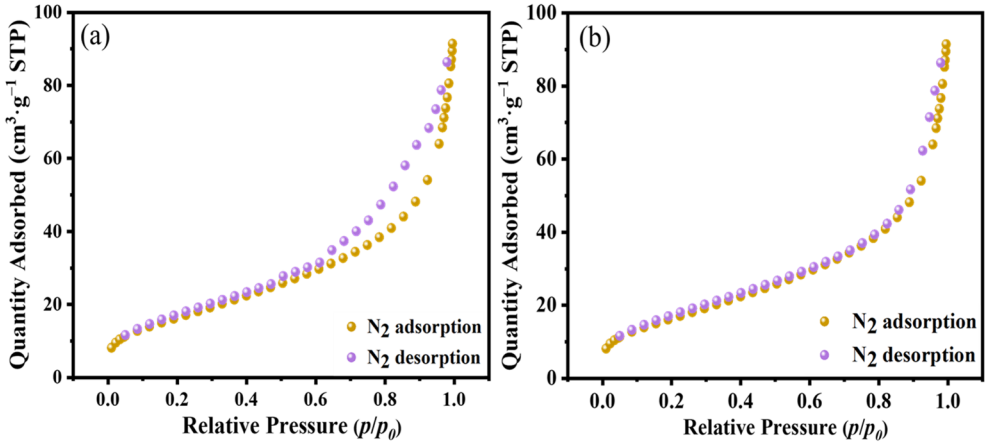

Figure 4. N_2 adsorption–desorption isotherms: (**a**) NS/Cd-IIP; (**b**) NS/Cd-NIP.

Table 1. Specific surface area and pore structure parameters of NS/Cd-IIP and NS/Cd-NIP.

Sample	Specific Surface Area ($m^2 \cdot g^{-1}$)	Pore Volume ($cm^3 \cdot g^{-1}$)	Average Pore Diameter (nm)
NS/Cd-IIP	65.19	0.177	8.495
NS/Cd-NIP	50.25	0.218	9.913

3.1.3. UV–Vis Analysis

To verify the coordination between Cd(II) and AM, a 1:4 Cd(II)–AM solution was prepared, and the absorbance of Cd(II) solution, AM solution, and Cd(II)–AM solution was measured, respectively. The results are depicted in Figure 5, where the maximum absorption peaks for Cd(II), AM, and 1:4 Cd(II)–AM solutions were observed at 204 nm, 213 nm, and 228 nm, respectively. If Cd(II) and AM do not coordinate, no new absorption peak will emerge. Instead, the absorption peak will overlap with that of Cd(II) and AM. Meanwhile, the red shift in the absorption peak of the 1:4 Cd(II)–AM solution indicates a charge transfer between the metal ion and ligand atoms. This is mainly due to the transition of lone pair electrons in N and O. Therefore, it indicates that Cd(II) coordinates with AM [23].

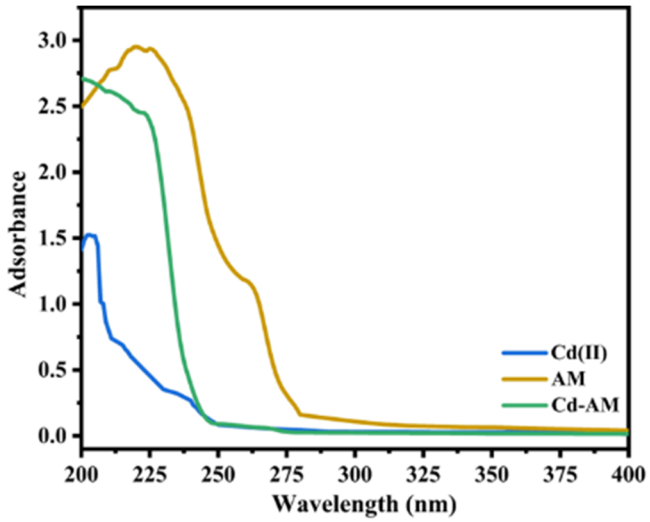

Figure 5. UV–vis spectra of Cd(II), AM solution, and Cd(II)–AM complex.

3.1.4. FTIR Analysis

The infrared spectra were analyzed to determine the functional groups in NS/Cd-IIP and NS/Cd-NIP. The results are presented in Figure 6. The broad peak observed at 3200–3500 cm^{-1} is attributed to the overlapping stretching vibration of –OH and N–H. The absorption peak at 2958 cm^{-1} corresponds to the stretching vibration peak of C−H bonds. The absorption peak at 1633 cm^{-1} is the characteristic peak of C=C in acrylamide. The absorption peak at 1475 cm^{-1} is caused by the bending vibration in the N–H plane of amide II [24]. The absorption peak at 1155 cm^{-1} indicates the Si–O–Si stretching vibration, and the absorption peak at 464 cm^{-1} is attributed to Si–OH vibration. In the NS/Cd-IIP infrared spectrum, the absorption peak at 1488 cm^{-1} is the in-plane bending vibration of the amide II band, and the absorption peak at 1730 cm^{-1} is attributed to –CO [25]. A red shift is observed in the imprinted composite, indicating coordination between cadmium ions and N and O atoms within the functional group, as compared to the non-imprinted composite. The changes in chemical shift and intensity of functional groups in NS/Cd-IIP further confirm the occurrence of the imprinting process.

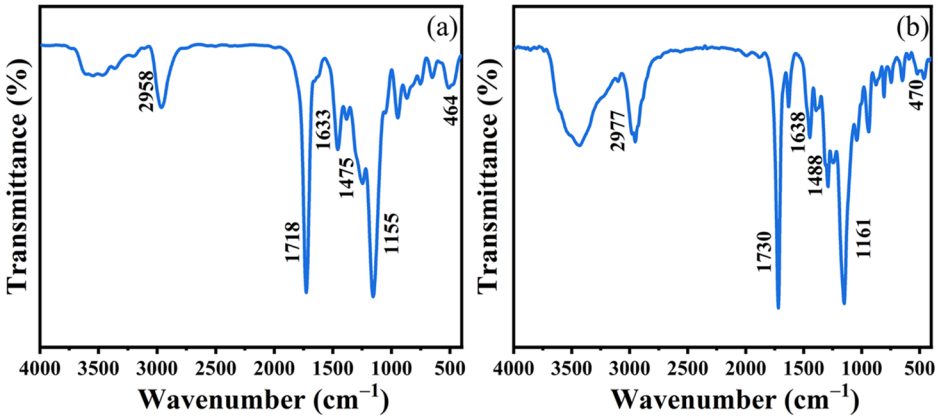

Figure 6. IR spectra of NS/Cd-NIP (**a**) and NS/Cd-IIP (**b**).

3.1.5. XPS Analysis

The NS/Cd-IIP and NS/Cd-NIP were characterized and analyzed using XPS, with the results presented in Figure 7. The full spectrum scanning is shown in Figure 7a, which reveals the presence of C, N, O, and Si in both NS/Cd-IIP and NS/Cd-NIP. In Figure 7b, the Si 2p energy spectrum of NS/Cd-IIP shows peaks at 103.7 eV, 102.7 eV, and 102.1 eV, corresponding to Si–OH, Si–O, and Si–C bonds, respectively, indicating that the cadmium ion-imprinted polymer is loaded on the natural sand. Figure 7c displays the N 1s energy spectrum of NS/Cd-NIP, with the peak at 399.6 eV attributed to $–NH_2$. Figure 7d displays the O 1s energy spectrum of NS/Cd-NIP, with two peaks at 532.0 eV and 531.8 eV assigned to $–CO–NH_2$ and Si–O–Si, respectively. In comparison with NS/Cd-NIP, both the $–NH_2$ peak in the N 1s energy spectrum shown in Figure 7e, and the $–CO–NH_2$ peak in the O 1s energy spectrum shown in Figure 7f exhibit an increase in binding energy for NS/Cd-IIP [26]. This phenomenon is due to the coordination between functional groups and Cd(II). Therefore, the cadmium ion-imprinted composite material with sand as the carrier was successfully prepared.

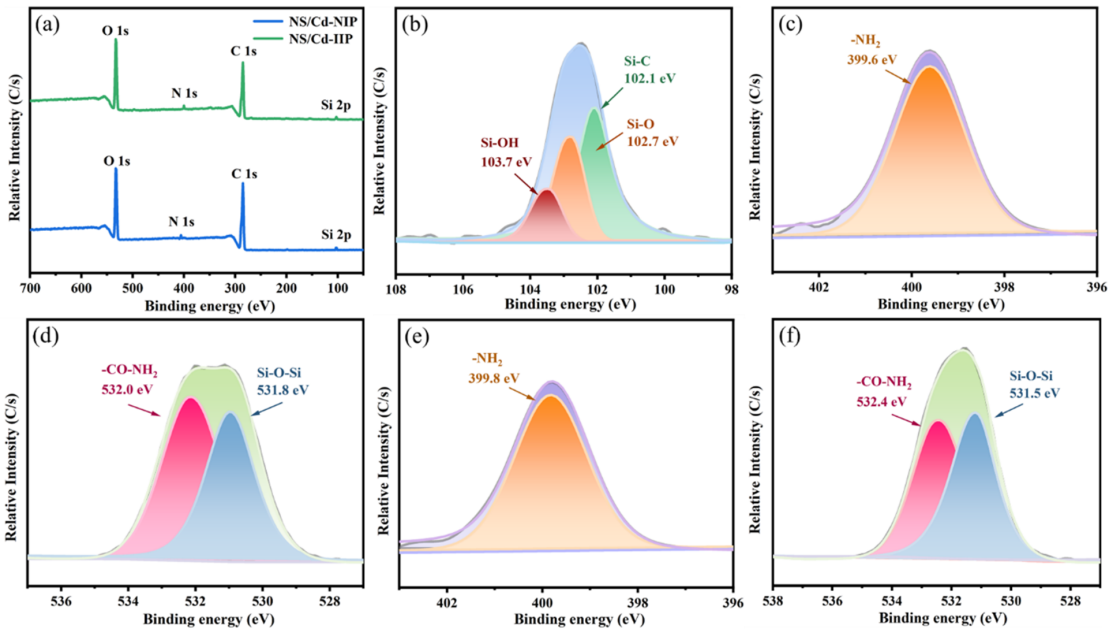

Figure 7. XPS spectra: (**a**) full spectrum; (**b**) Si 2p spectrum of NS/Cd-IIP; (**c**) N 1s spectrum of NS/Cd-NIP; (**d**) O 1s spectrum of NS/Cd-NIP; (**e**) N 1s spectrum of NS/Cd-IIP; (**f**) O 1s spectrum of NS/Cd-IIP.

3.2. Static Adsorption Experiments

3.2.1. Effect of Different Factors on Adsorption

Effect of pH

The pH value of the metal ion solution is a variable that affects the adsorption process. This study investi.gates the influence of NS/Cd-IIP on Cd(II) adsorption in the pH range of 1–10, as depicted in Figure 8a. The adsorption rate gradually increases within the pH range of 1–7 and then decreases with rising pH. This phenomenon occurs because the functional groups of NS/Cd-IIP are protonated to different degrees, and the H^+ content of the solution is varying at different acidity levels. In acidic conditions, Cd(II) primarily exists as cations in the aqueous phase. Because of the competition for adsorption sites between H^+ and these cations, the competition from H^+ is greater than that of Cd(II). With an increase in pH, the concentration of OH^- rises, resulting in the formation of Cd(II) as hydroxides [27]. Functional monomer groups become deprotonated, leading to reduced adsorption capacity.

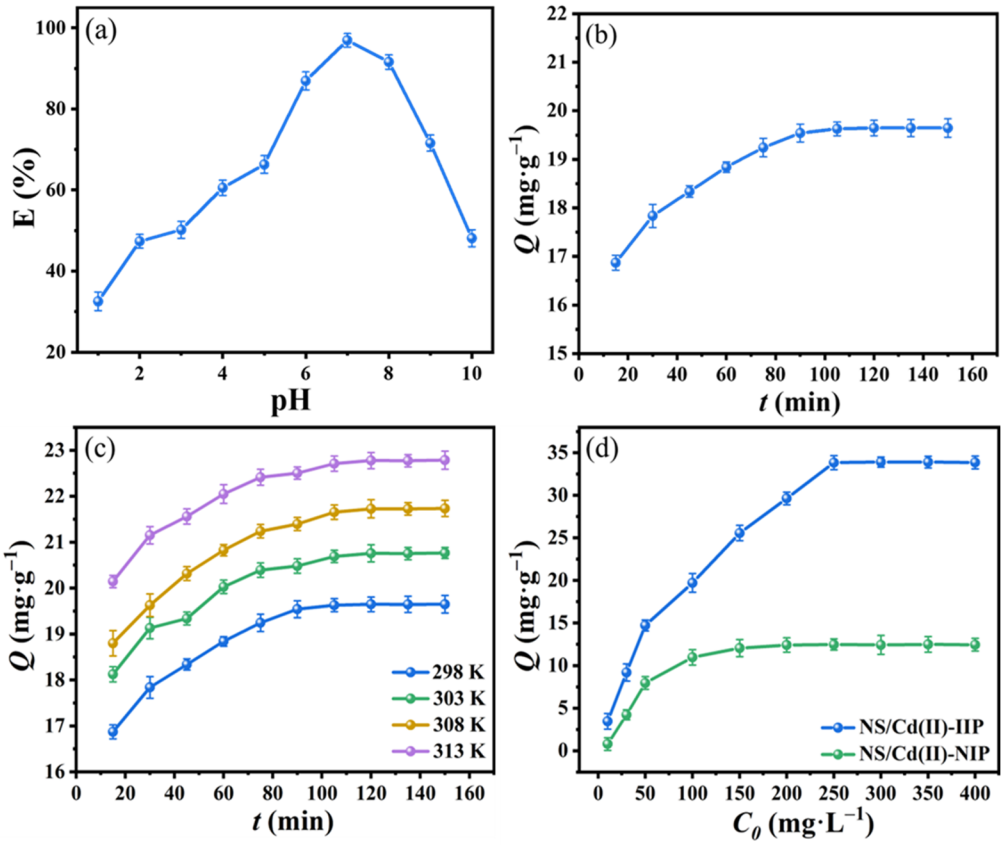

Figure 8. The effect of different factors on adsorption properties in static adsorption experiment: (**a**) pH value; (**b**) time; (**c**) temperature; (**d**) initial solution concentration (experimental conditions: C_0 = 100 mg·L^{-1}; sample volume: 10 mL; time: 105 min; pH: 7; temperature: 298 K).

Effect of Contact Time

To determine the adsorption time of Cd(II) by NS/Cd-IIP, the results are presented in Figure 8b. With increasing time, the adsorption capacity of NS/Cd-IIP for Cd(II) gradually increased. When the adsorption sites on the surface of the composite were gradually occupied, equilibrium was reached at 105 min. During the initial stage of adsorption, Cd(II) selectively bound to the specific recognition sites of the imprinted polymer, resulting in a faster adsorption rate. However, in later stages, surface adsorption and diffusion dominated, leading to a slower adsorption rate. Furthermore, NS/Cd-IIP reached equilibrium earlier than NS/Cd-NIP due to its imprinted sites on the surface, which enhanced the adsorption for Cd(II) [28].

Effect of Temperature

The effect of NS/Cd-IIP on the adsorption performance of Cd(II) was studied in the temperature range of 298–313 K. Parameters of the thermodynamics during adsorption were calculated according to Equations (12) and (13) [29].

$$\Delta G^0 = -RT\ln K_d \tag{12}$$

$$\ln K_d = -\frac{\Delta H^0}{RT} + \frac{\Delta S^0}{R} \tag{13}$$

where K_d is the equilibrium constant, R is the ideal gas constant, ΔG^0 ($kJ \cdot mol^{-1}$) is the Gibbs free energy, ΔH^0 ($kJ \cdot mol^{-1}$) is the enthalpy change, ΔS^0 ($J \cdot mol^{-1} \cdot k^{-1}$) is the entropy change, and T (K) is the temperature.

The results depicted in Figure 8c indicate that as temperature increased, the adsorption capacity of NS/Cd-IIP for Cd(II) rose from 19.63 $mg \cdot g^{-1}$ to 22.71 $mg \cdot g^{-1}$. In this temperature range, higher temperatures are more conducive to the adsorption for Cd(II), possibly due to the increased stability of template ions interacting with functional monomer groups when the temperature is from 298 K to 313 K. The thermodynamic parameters of Cd(II) adsorption by NS/Cd-IIP are presented in Table 2. The negative value of ΔH^0 indicates an exothermic process, while the positive value of ΔS^0 suggests that the adsorption is accompanied by an increase in entropy [30]. Moreover, the negative value of ΔG^0 indicates a spontaneous process.

Table 2. Thermodynamic parameters of NS/Cd-IIP.

ΔG^0 ($kJ \cdot mol^{-1}$)				ΔS ($J \cdot mol^{-1} \cdot K^{-1}$)	ΔH^0 ($kJ \cdot mol^{-1}$)
298 K	**303 K**	**308 K**	**313 K**		
−5.417	−5.431	−5.445	−5.459	2.801	−4.583

Effect of Initial Concentration

The effect of initial solution concentration on adsorption performance was investigated. The results are presented in Figure 8d. As the initial concentration increased, both NS/Cd-IIP and NS/Cd-NIP exhibited a gradual increase in adsorption capacity for Cd(II), which eventually stabilized at saturation. At various initial concentrations, NS/Cd-IIP exhibited significantly higher adsorption capacity for Cd(II) than NS/Cd-NIP. The saturated adsorption capacity of NS/Cd-NIP and NS/Cd-IIP were 12.04 $mg \cdot g^{-1}$ and 33.84 $mg \cdot g^{-1}$, respectively. The superior adsorption performance of NS/Cd-IIP can be attributed to the specific binding sites on the surface of eluted template ions and geometrically matched imprinted hole size for Cd(II). The non-imprinted polymer lacks specific imprinting sites on its surface, resulting in relatively weak adsorption capacity.

3.2.2. Adsorption Kinetic

In order to further study the adsorption process, quasi-first-order and quasi-second-order kinetic models were used to fit the adsorption of Cd(II) by NS/Cd-IIP at different temperatures, respectively, and the linear correlation coefficients and corresponding rate constants were obtained. The kinetic equations are shown in Equations (14) and (15) [31]:

$$\ln(Q_e - Q_t) = \ln Q_e - k_1 t \tag{14}$$

$$\frac{t}{Q_t} = \frac{k_2}{Q_e^2} + \frac{t}{Q_e} \tag{15}$$

where Q_e ($mg \cdot g^{-1}$) and Q_t ($mg \cdot g^{-1}$) are the adsorption capacity at adsorption equilibrium and time t, respectively. k_1 and k_2 are the rate constants of the quasi-first-order and quasi-second-order kinetic equations, respectively.

The nonlinear fit of the kinetic is shown in Figure 9, and the kinetic model parameters are shown in Table 3. The results show that the quasi-second-order kinetic model has a higher linearity than the quasi-first-order kinetic model, indicating that the model is more suitable for describing the adsorption process. In addition, it can more accurately estimate the actual adsorption amount. Therefore, it can be concluded that the adsorption of Cd(II) by NS/Cd-IIP belongs to a chemical process, mainly the interaction between AM functional groups and Cd(II).

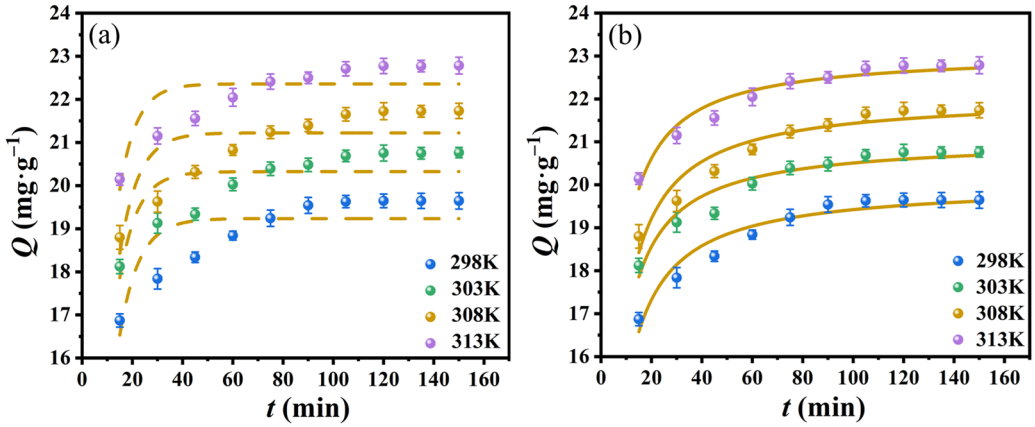

Figure 9. Quasi-first-order (**a**) and quasi-second-order kinetic model (**b**) fitting at different temperatures.

Table 3. Kinetic model parameters of NS/Cd-IIP at different temperatures.

T (K)	Quasi-First-Order			Quasi-Second-Order		
	$Q_{e,cal}$ $mg \cdot g^{-1}$	k_1 min^{-1}	R^2	$Q_{e,cal}$ $mg \cdot g^{-1}$	k_2 min^{-1}	R^2
298	19.23	0.131	0.67	20.03	0.016	0.96
303	20.32	0.135	0.65	21.06	0.017	0.95
308	21.22	0.141	0.63	22.07	0.015	0.93
313	22.36	0.147	0.67	23.08	0.018	0.95

3.2.3. Adsorption Isotherm

In order to investigate the adsorption behavior of NS/Cd-IIP and NS/Cd-NIP towards Cd(II), we modeled the experimental adsorption process using Langmuir and Freundlich isotherms. The Langmuir isotherm model assumes monolayer adsorption on a homogeneous surface with a fixed number of binding sites, which are considered to have equal energy and are separated by a certain distance. Therefore, the interaction between the adsorbed molecules is neglected [32]. The nonlinear equation of the Langmuir isothermal model is as follows:

$$Q_e = \frac{Q_m K_L C_e}{1 + K_L C_e} \quad (16)$$

where K_L is the Langmuir adsorption constant.

To assess the feasibility of adsorption, the fundamental characteristics of the Langmuir isotherm equation can be elucidated by a dimensionless parameter known as the separation factor R_L, which can be mathematically defined as follows:

$$R_L = \frac{1}{1 + K_L C_0} \quad (17)$$

If $R_L > 1$, the adsorption is unfavorable. If $R_L = 1$, the adsorption isotherm follows a linear trend. If $R_L < 1$, the adsorption is favorable. If $R_L = 0$, the adsorption is irreversible.

The Freundlich isotherm equation is an empirical equation for multi-layer adsorption, where the energy of each adsorption site varies. The nonlinear equation of the Freundlich isotherm model is as follows:

$$Q_e = K_F C_e^{\frac{1}{n}} \quad (18)$$

where K_F is the Freundlich adsorption constant.

A smaller value of 1/n indicates a higher degree of surface heterogeneity in the adsorbent, while a value closer to 1 suggests a greater homogeneity in the distribution of adsorption sites on the surface.

The fitting results of the adsorption process are shown in Figure 10, and the fitted adsorption isotherm parameters are shown in Table 4. The R^2 values of the Langmuir isothermal model were larger than those of the Freundlich isothermal model. The adsorption capacity calculated using the Langmuir isotherm is close to the actual value. Therefore, the adsorption behavior of NS/Cd-NIP on Cd(II) is more consistent with the Langmuir isotherm, which belongs to the monolayer adsorption. In addition, the R_L was calculated between 0 and 1, indicating that adsorption was favorable [32].

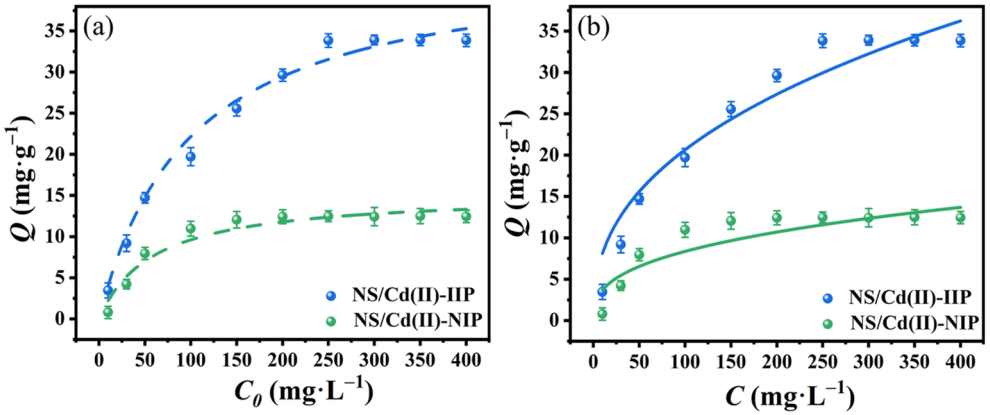

Figure 10. Adsorption isotherm curves of NS/Cd-IIP and NS/Cd-NIP: (**a**) Langmuir isotherm; (**b**) Freundlich isotherm.

Table 4. Langmuir and Freundlich isotherm parameters for NS/Cd-NIP.

Adsorbent	Langmuir Isotherm				Freundlich Isotherm		
	K_L	Q_m (mg·g^{-1})	R^2	R_L	K_F	1/n	R^2
NS/Cd-IIP	0.026	36.33	0.99	0.13	7.10	0.27	0.89
NS/Cd-NIP	0.017	15.28	0.95	0.28	1.63	0.36	0.85

3.2.4. Adsorption Selectivity

The results of the selectivity experiment are presented in Figure 11, while the calculation results of selectivity parameters are shown in Table 5. The selectivity of NS/Cd-IIP for Cd(II) is significantly higher than that for Cu(II), Mn(II), Ni(II), and Pb(II). As the imprinted cavities on the surface of the ion-imprinted composite match with Cd(II), the active sites on its surface interact preferentially with Cd(II) [33]. Consequently, NS/Cd-IIP exhibits a stronger affinity towards Cd(II) and thus displays high selectivity for it.

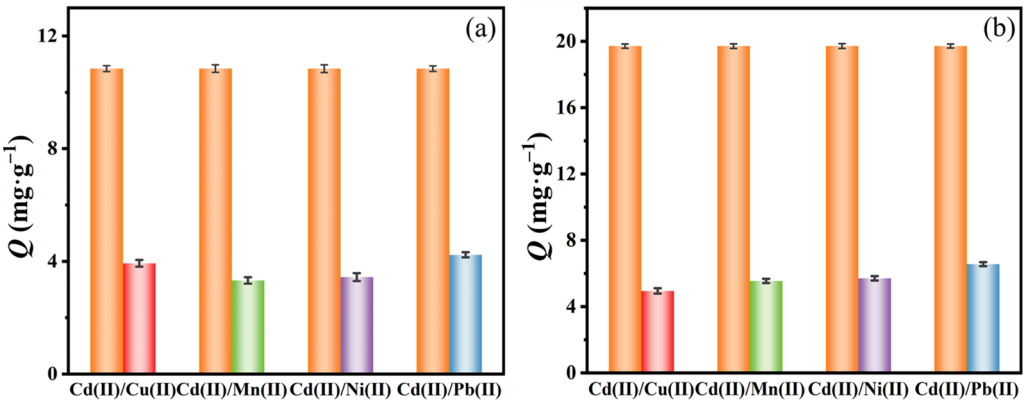

Figure 11. Selective adsorption of Cd(II) by NS/Cd-NIP (**a**) and NS/Cd-IIP (**b**) (experimental conditions: C_0 = 100 mg·L^{-1}; sample volume: 10 mL; time: 105 min; pH: 7; temperature: 298 K).

Table 5. Selectivity parameters of NS/Cd-IIP and NS/Cd-NIP for Cd(II).

M(II)	D		α		k
	IIP	NIP	IIP	NIP	
Cd(II)	13.601	0.236	-	-	-
Cu(II)	0.066	0.0521	207.0	4.53	45.70
Mn(II)	0.077	0.0459	170.3	5.14	33.13
Ni(II)	0.080	0.0481	170.4	4.91	34.70
Pb(II)	0.098	0.0633	139.5	3.73	37.40

3.3. Dynamic Adsorption Experiments

3.3.1. Breakthrough Curves under Different Conditions

Breakthrough Curves of NS/Cd-IIP and NS/Cd-NIP

The breakthrough curves of NS/Cd-IIP and NS/Cd-NIP are shown in Figure 12a. The parameters of the adsorption process are shown in Table 6. The dynamic adsorption capacities of NS/Cd-IIP and NS/Cd-NIP for Cd(II) were determined to be 1.32 mg·g^{-1} and 0.25 mg·g^{-1}, respectively. However, under the same conditions (Cd(II) solution concentration of 10 mg·L^{-1}), the dynamic adsorption capacity was found to be lower than the static adsorption capacity. This could possibly be attributed to insufficient contact time between the adsorbents and Cd(II) solution during the dynamic adsorption process.

Influence of Microcolumn Filling Height on the Breakthrough Curve

To investigate the impact of microcolumn adsorbent height on dynamic adsorption, three different heights were selected for testing at the same loading flow rate and initial solution concentration. The results are shown in Figure 12b. As the height of the adsorbent increases, the breakthrough time during the adsorption process lengthens, resulting in a prolonged time to reach adsorption equilibrium and an increase in the total adsorption amount. Due to the increased mass transfer area, there is more contact time between the adsorbent and adsorbate [34]. The increased height of the microcolumn and mass of the adsorbent lead to an increase in both the active area for ion adsorption and binding, thereby enhancing its ability to adsorb Cd(II).

Influence of Initial Concentration on the Breakthrough Curve

The impact of the initial Cd(II) concentration on dynamic adsorption is presented in Figure 12c. As the initial concentration increases, both the breakthrough time and the time to reach adsorption equilibrium decrease, while the adsorption capacity increases. With an increase in solution concentration, the mass transfer resistance of Cd(II) from the liquid phase to the imprinted polymer is reduced. This reduction leads to a stronger driving force and an enhanced adsorption capacity [35].

Influence of Flow Rate on the Breakthrough Curve

In order to investigate the impact of Cd(II) solution flow rate on dynamic adsorption, various flow rates were controlled during dynamic adsorption experiments. The results are presented in Figure 12d, which indicate that a faster flow rate leads to a steeper slope in the breakthrough curve. The adsorption equilibrium time decreased from 55 to 35 min due to the increased flow rate, which resulted in a shorter contact time between the adsorbent and the adsorbate. This limited the diffusion of Cd(II) on the surface of NS/Cd-IIP as it passed through the adsorption microcolumn, ultimately leading to a decreased adsorption capacity [36].

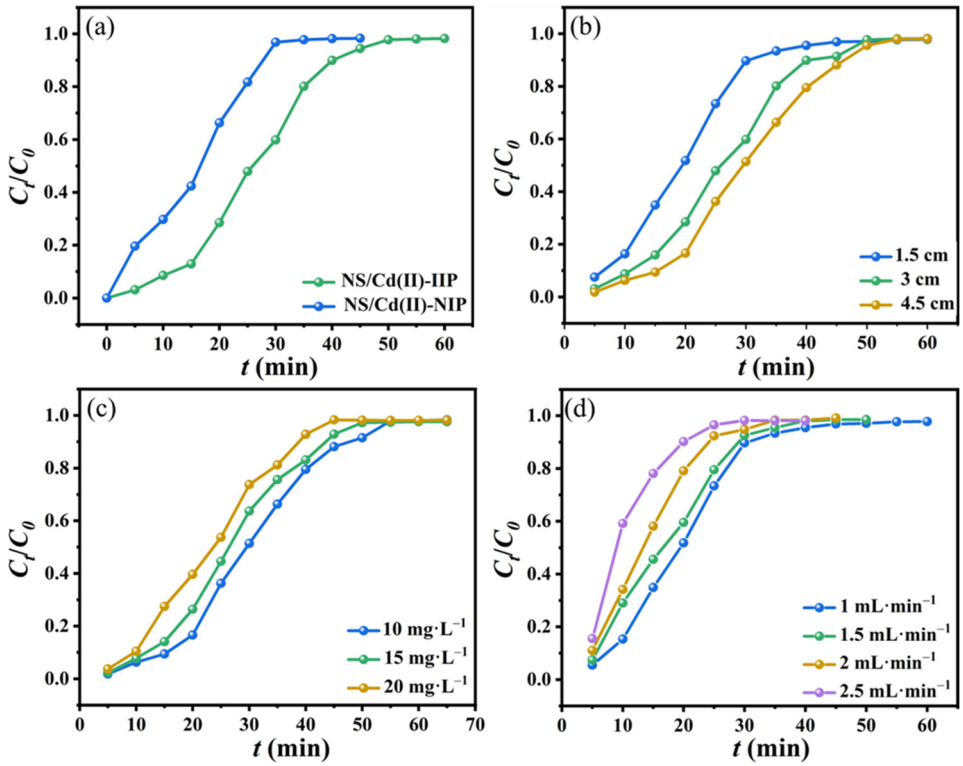

Figure 12. Dynamic adsorption penetration curves under different conditions: (**a**) adsorbent; (**b**) the filling height of the microcolumn; (**c**) initial solution concentration; (**d**) loading flow rate (experimental conditions: C_0 = 10 mg·L^{-1}; pH: 7; flow rate: 1 mL·min^{-1}; temperature: 298 K).

Table 6. Parameters in dynamic adsorption experiment for Cd(II) adsorption by NS/Cd-IIP.

C_0 mg·L^{-1}	Z cm	V mL·min^{-1}	t_b min	t_e min	V_e L	q_e mg·g^{-1}	q_{total} mg
10	1.5	1	10	45	0.045	2.32	0.023
10	3	1	15	50	0.050	1.29	0.026
10	4.5	1	20	55	0.055	0.98	0.029
10	1.5	1	10	45	0.045	2.32	0.023
10	1.5	1.5	8	40	0.035	1.94	0.019
10	1.5	2	5	35	0.025	1.24	0.012
10	1.5	2.5	3	30	0.020	0.97	0.097
10	4.5	1	20	55	0.055	0.98	0.029
15	4.5	1	15	50	0.050	2.36	0.071
20	4.5	1	10	45	0.045	3.77	0.113

3.3.2. Dynamic Adsorption Model

The Adams–Bohart model postulates that the attainment of adsorption equilibrium is not instantaneous and that the rate of adsorption depends on both the concentration of the adsorbate and the remaining capacity for adsorption on the adsorbent. This model is employed to fit various conditions in the adsorption process, as depicted in Figure 13, with diverse parameters presented in Table 7 after computation. The results indicate that faster adsorption rates can be achieved at lower filling heights, smaller initial concentrations, and higher loading flow rates. However, theoretical values fitted by the Adams–Bohart model significantly differ from experimental data, indicating that this model is not suitable to describe the adsorption process of NS/Cd-IIP for Cd(II).

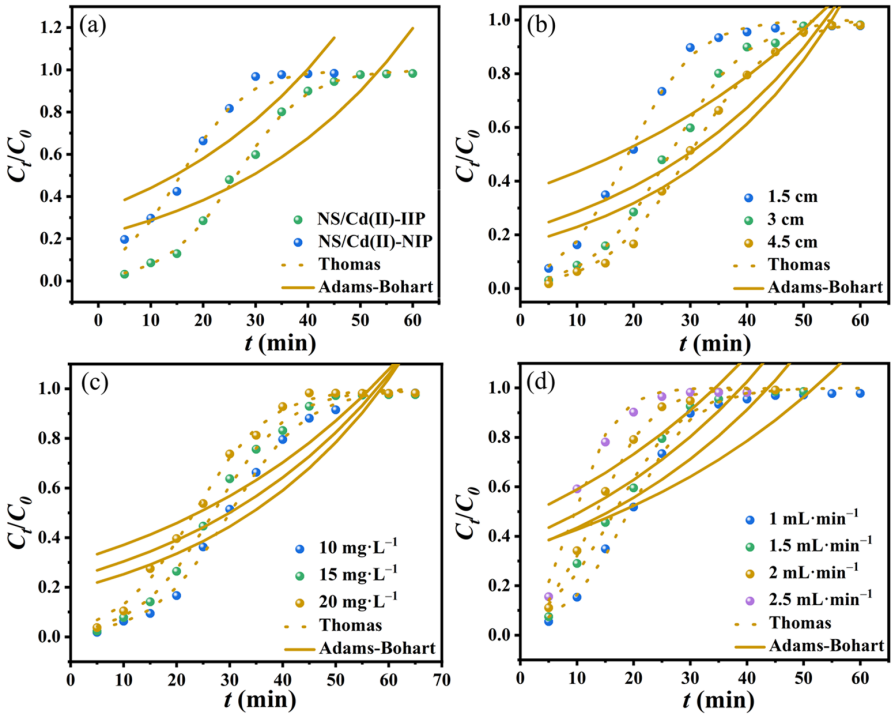

Figure 13. Fitting of Adams–Bohart and Thomas model for dynamic adsorption penetration curves under different conditions: (**a**) adsorbent; (**b**) the filling height of the microcolumn; (**c**) initial solution concentration; (**d**) loading flow rate.

Table 7. Parameters of Adams–Bohart model.

Parameters Varied	K_{AB} (mL·min^{-1}·mg^{-1})	N_0 (mg·mL^{-1})	R^2
Column depth (cm)			
1.5	3.28	0.749	0.692
3	2.86	0.538	0.801
4.5	1.99	0.518	0.861
Initial concentration (mg·L^{-1})			
10	2.59	0.105	0.792
15	1.41	0.158	0.783
20	0.98	0.572	0.821
Flow rate (mL·min^{-1})			
1	3.12	0.545	0.856
1.5	3.24	0.506	0.824
2	3.28	0.487	0.803
2.5	3.51	0.462	0.686

The Thomas model assumes that the adsorption process conforms to the Langmuir isotherm and quasi-second-order kinetic model while neglecting axial diffusion [37]. It has been applied to fit the adsorption under various conditions, with results which are presented in Figure 13. Table 8 displays the calculated parameters. These results indicate that the dynamic adsorption process is better described by the Thomas model.

Table 8. Parameters of Thomas model.

Parameters Varied	K_{Th} (mL·min^{-1}·mg^{-1})	q (mg·g^{-1})	R^2
Column height (cm)			
1.5	17.05	1.90	0.971
3	14.90	1.32	0.987
4.5	13.72	0.99	0.992
Initial concentration (mg·L^{-1})			
10	14.23	1.33	0.979
15	7.84	2.39	0.983
20	4.89	3.81	0.991
Flow rate (mL·min^{-1})			
1	14.14	2.33	0.992
1.5	15.11	1.96	0.988
2	17.23	1.31	0.984
2.5	17.96	1.01	0.969

3.4. Optimization of Elution Parameters

3.4.1. Influence of Eluent Type and Concentration on Desorption

Under acidic conditions, the functional groups of imprinted polymers can be protonated and replaced by metal ions. To desorb Cd(II) adsorbed on NS/Cd-IIP, common desorption agents such as HCl, HNO_3, and H_2SO_4 are typically used. In this study, we selected these three acids at equal concentrations as eluents. The results shown in Figure 14a demonstrate that all three acid solutions effectively eluted Cd(II). Among the 3 acids, HCl exhibited the highest elution efficiency, with a desorption rate of 95.4%. This could be attributed to the strong coordination effect between Cd(II) and Cl^-, making HCl an optimal choice as a desorbing agent [38].

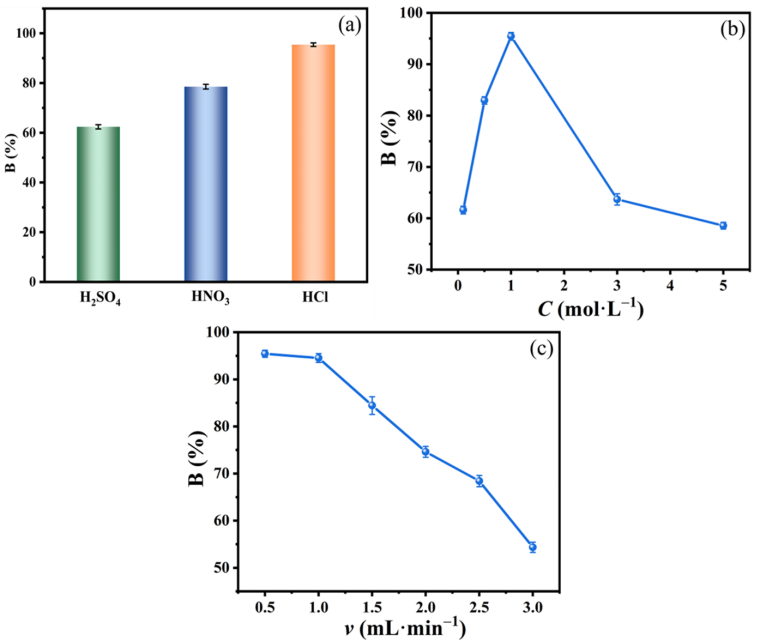

Figure 14. Effect of eluent on desorption: (**a**) type of eluent; (**b**) concentration of eluent; (**c**) flow rate of eluent.

3.4.2. Effect of Eluent Flow Rate on Desorption

To further optimize the desorption conditions, an investigation was conducted on the effect of different desorption flow rates on elution efficiency. The results are presented in Figure 14c. With an increase in flow rate, the desorption effect gradually weakened. At a flow rate of 1 mL·min^{-1}, the desorption rate reached 95.4%. When the flow rate is high, the desorption effect is relatively weak due to the short contact time between the desorption solution and Cd(II) on the adsorbent surface. H^+ does not have sufficient time to displace Cd(II) from the composite material surface [39]. Therefore, considering all factors, a flow rate of 1mL·min^{-1} for the desorption solution was selected.

3.5. Adsorption Mechanism

To investigate the adsorption mechanism of Cd(II), FTIR and XPS analyses were conducted on NS/Cd-IIP after adsorption. The peak intensity and position of the composite material changed significantly, as depicted in Figure 15a. Compared to the infrared spectra prior to adsorption, the N–H absorption peak shifted from 1488 cm^{-1} to 1498 cm^{-1}, and the –CO absorption peak shifted from 1730 cm^{-1} to 1735 cm^{-1}, indicating that functional groups provided adsorption sites for Cd(II). Figure 15b displays the full spectrum scan of NS/Cd-IIP; the absorption peaks of C, N, O, and Si are observed in both imprinted composite before and after adsorption. Additionally, a Cd absorption peak is detected in the spectrum after adsorption, indicating the successful adsorption of Cd(II) on NS/Cd-IIP. The N 1s energy spectrum in Figure 15c indicates that the binding energy of $-NH_2$ shifts from 399.8 eV to 400.6 eV after adsorption, which is attributed to the coordination between the N atom and Cd(II). Moreover, Figure 15d of the O 1s energy spectrum reveals that the binding energy of –CO–NH_2 changes from 532.4 eV to 533.3 eV after adsorption, providing evidence for the interaction between N and O atoms with Cd(II) [40].

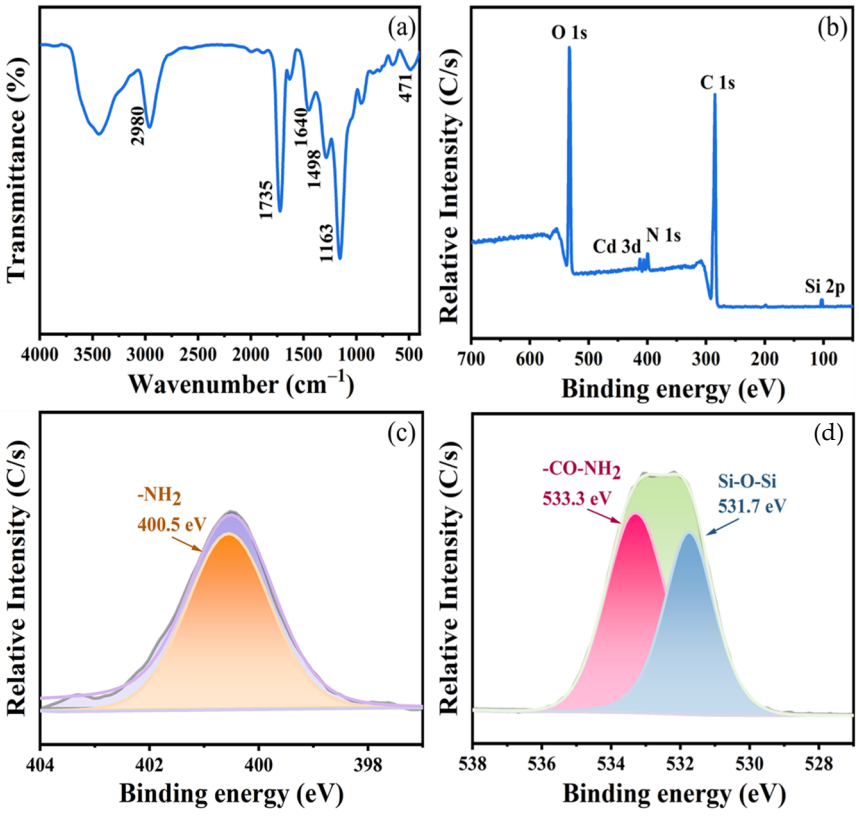

Figure 15. IR spectra of NS/Cd-IIP after adsorption Cd(II) (**a**); XPS full spectrum (**b**); N 1s spectrum (**c**); O 1s spectrum (**d**).

The adsorption sites were determined through the plotting of surface electrostatic potential, as shown in Figure 16, where the electrostatic potential decreases from red to blue. At the molecular surface, atoms with more negative electrostatic potential are more likely to donate electrons for electrophilic reactions [41]. The isosurface figure shows that the minimum point of electrostatic potential around AM is located near the O atom in the C=O group, indicating a tendency for this atom to contribute its lone pair of electrons to coordinate with Cd(II) [42]. The electrostatic potential surrounding the N atom of the $-NH_2$ group is relatively negative, indicating its involvement in coordinating Cd(II) ions. A schematic of the adsorption mechanism is shown in Figure 17.

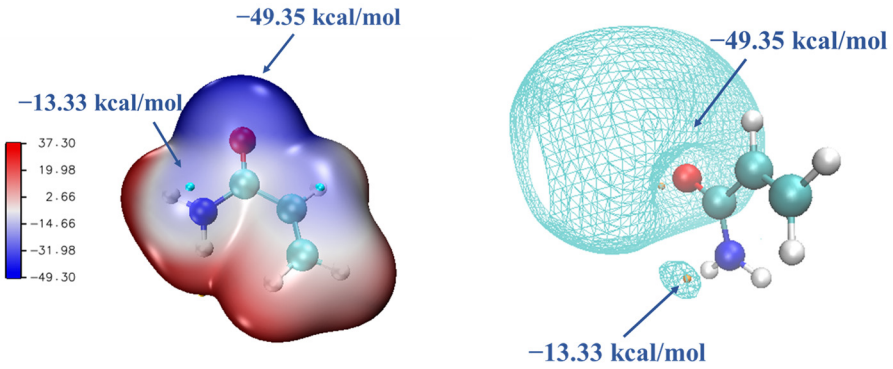

Figure 16. ESP and isosurface of the AM surface.

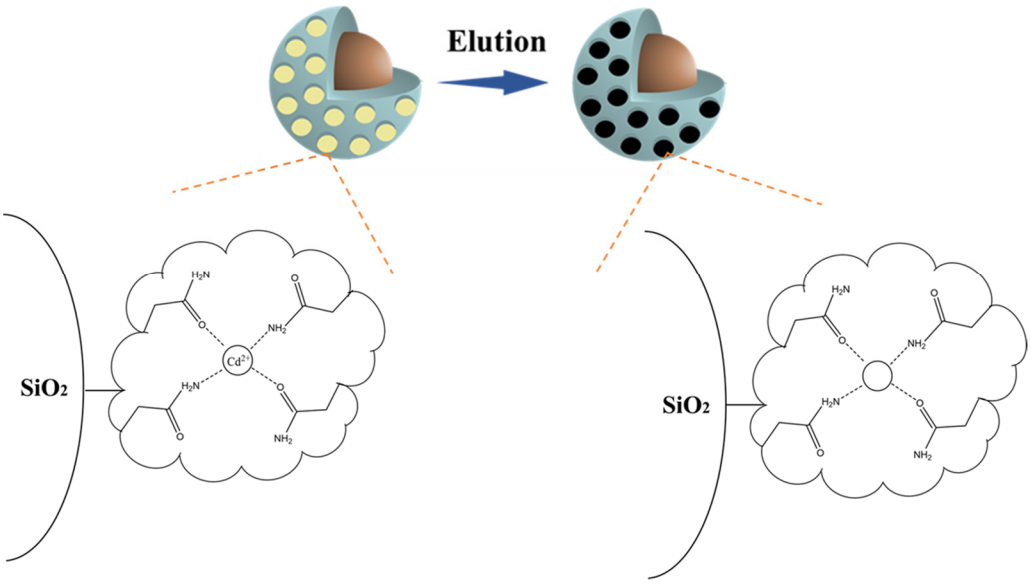

Figure 17. Schematic of the adsorption mechanism.

3.6. Reusability of NS/Cd-IIP

The reusability of adsorbents is important for maximizing their economic benefits. NS/Cd-IIP was desorbed with 1 $mol \cdot L^{-1}$ hydrochloric acid at the end of the adsorption experiment, followed by the repetition of the adsorption–desorption cycle. The results, as shown in Figure 18, indicate that the adsorption capacity of NS/Cd-IIP for Cd(II) decreases to 10.39 $mg \cdot g^{-1}$ after eight cycles, which still exhibits favorable adsorption performance and demonstrates the excellent reusability of NS/Cd-IIP.

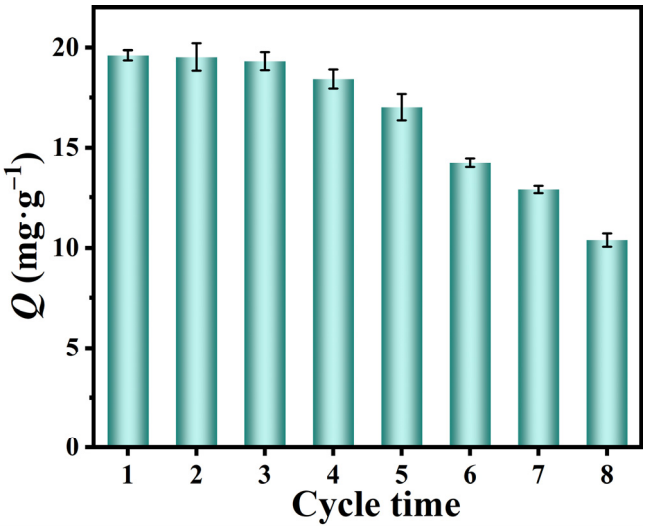

Figure 18. Reusability of NS/Cd-IIP.

3.7. Analysis of Actual Water Samples

The prepared NS/Cd-IIP was used as a solid-phase extraction material for the preconcentration and determination of trace cadmium ions in actual water samples. The standard addition method was employed to analyze the water samples, and the results are shown in Table 9. The experimental results demonstrate that NS/Cd-IIP can be effectively utilized for the preconcentration of Cd(II) in water samples, as evidenced by the recovery rates exceeding 101% when 5 μg·L^{-1} and 10 μg·L^{-1} Cd(II) were added to tap water.

Table 9. Determination of Cd(II) in tap water.

Sample	Added (μg·L^{-1})	Found (μg·L^{-1})	Recovery %
Tap water	0	0.13 ± 0.02	-
	5.00	5.32 ± 0.16	103.8 ± 2.8
	10.00	10.23 ± 0.18	101.1 ± 1.7

4. Conclusions

In this study, a cadmium-imprinted/natural sand composite was prepared using surface imprinting techniques. The composite was characterized using UV–vis, FTIR, SEM, EDS, and XPS analyses, which confirmed the successful preparation of the composite. The adsorption behavior of both NS/Cd-IIP and NS/Cd-NIP was fitted to the Langmuir adsorption isotherm. The adsorption process of NS/Cd-IIP at different temperatures conformed to the quasi-second-order kinetic equation, indicating that it involved a chemical process. Thermodynamic parameters revealed that the adsorption of Cd(II) by NS/Cd-IIP was an exothermic, entropic, and spontaneous process. The results demonstrated that NS/Cd-IIP exhibited high selectivity for Cd(II). The dynamic adsorption capacity was found to be inferior to the static adsorption capacity under the same conditions. The adsorption process of NS/Cd-IIP for Cd(II) was consistent with the Thomas model. The results of the adsorption and desorption cycle experiments demonstrated that NS/Cd-IIP exhibited excellent regeneration performance. Coordination between N and O atoms and Cd(II) primarily characterized the adsorption of Cd(II) by NS/Cd-IIP.

Author Contributions: Conceptualization, A.M.; methodology, A.M.; investigation, A.M.; writing—original draft preparation, A.M.; data curation, S.G.; writing—review and editing, S.A. and A.Y.; visualization, L.W. and L.C.; supervision, S.A. All authors have read and agreed to the published version of the manuscript.

Funding: This research was funded by National Natural Science Foundation of China grant number 52163030.

Institutional Review Board Statement: Not applicable.

Informed Consent Statement: Not applicable.

Data Availability Statement: Not applicable.

Acknowledgments: The authors would like to thank the National Natural Science Foundation of China (No. 52163030) for funding this research.

Conflicts of Interest: The authors declare no conflict of interest.

References

1. Jadoun, S.; Fuentes, J.P.; Urbano, B.F.; Yáñez, J. A review on adsorption of heavy metals from wastewater using conducting polymer-based materials. *J. Environ. Chem. Eng.* **2023**, *11*, 109226. [CrossRef]
2. Briffa, J.; Sinagra, E.; Blundell, R. Heavy metal pollution in the environment and their toxicological effects on humans. *Heliyon* **2020**, *6*, e04691. [CrossRef]
3. Rusin, M.; Domagalska, J.; Rogala, D.; Razzaghi, M.; Szymala, I. Concentration of cadmium and lead in vegetables and fruits. *Sci. Rep.* **2021**, *11*, 11913. [CrossRef]
4. Kayranli, B. Cadmium removal mechanisms from aqueous solution by using recycled lignocelluloses. *Alex. Eng. J.* **2022**, *61*, 443–457. [CrossRef]
5. Rahman, Z.; Singh, V.P. The relative impact of toxic heavy metals (THMs) (arsenic (As), cadmium (Cd), chromium (Cr)(VI), mercury (Hg), and lead (Pb)) on the total environment: An overview. *Environ. Monit. Assess.* **2019**, *191*, 419. [CrossRef]
6. Qasem, N.A.A.; Mohammed, R.H.; Lawal, D.U. Removal of heavy metal ions from wastewater: A comprehensive and critical review. *Npj Clean Water* **2021**, *4*, 36. [CrossRef]
7. Nishide, H.; Tsuchida, E. Selective adsorption of metal ions on poly (4-vinylpyridine) resins in which the ligand chain is immobilized by crosslinking. *Die Makromol. Chem. Macromol. Chem. Phys.* **1976**, *177*, 2295–2310. [CrossRef]
8. Zhou, X.; Wang, B.; Wang, R. Insights into ion-imprinted materials for the recovery of metal ions: Preparation, evaluation and application. *Sep. Purif. Technol.* **2022**, *298*, 121469. [CrossRef]
9. Zhou, Z.; Kong, D.; Zhu, H.; Wang, N.; Wang, Z.; Wang, Q.; Liu, W.; Li, Q.; Zhang, W.; Ren, Z. Preparation and adsorption characteristics of an ion-imprinted polymer for fast removal of Ni(II) ions from aqueous solution. *J. Hazard. Mater.* **2018**, *341*, 355–364. [CrossRef]
10. Zhang, H.; Ma, R.; Yang, Y.; Huang, L.; Chen, N.; Xie, Q. Study of ion-imprinted adsorbent materials on diatom-based Cr(VI) Surfaces. *Mater. Lett.* **2022**, *308*, 131149. [CrossRef]
11. Huang, R.; Shao, N.; Hou, L.; Zhu, X. Fabrication of an efficient surface ion-imprinted polymer based on sandwich-like graphene oxide composite materials for fast and selective removal of lead ions. *Colloids Surf. A Physicochem. Eng. Asp.* **2019**, *566*, 218–228. [CrossRef]
12. Yu, L.; Sun, L.; Zhang, Q.; Zhou, Y.; Zhang, J.; Yang, B.; Xu, B.; Xu, Q. Nanomaterials-Based Ion-Imprinted Electrochemical Sensors for Heavy Metal Ions Detection: A Review. *Biosensors* **2022**, *12*, 1096. [CrossRef] [PubMed]
13. Lv, X.; Huiyi, H.; Yao, L.; Deng, L.; Liu, X.; Yu, L.; He, H. Fabrication of surface ion imprinting rice husk-based polymer for selective detection and efficient adsorption of Cu2+ in lake water. *Spectrochim. Acta Part A Mol. Biomol. Spectrosc.* **2023**, *298*, 122723. [CrossRef]
14. Liu, W.; Zhang, M.; Liu, X.; Zhang, H.; Jiao, J.; Zhu, H.; Zhou, Z.; Ren, Z. Preparation of Surface Ion-Imprinted Materials Based on Modified Chitosan for Highly Selective Recognition and Adsorption of Nickel Ions in Aqueous Solutions. *Ind. Eng. Chem. Res.* **2020**, *59*, 6033–6042. [CrossRef]
15. Lu, J.; Wu, Y.; Lin, X.; Gao, J.; Dong, H.; Chen, L.; Qin, Y.; Wang, L.; Yan, Y. Anti-fouling and thermosensitive ion-imprinted nanocomposite membranes based on grapheme oxide and silicon dioxide for selectively separating europium ions. *J. Hazard. Mater.* **2018**, *353*, 244–253. [CrossRef]
16. Ma, R.; Yang, Y.; Zhang, X.; Fu, B.; Li, X.; Huang, L.; Chen, N.; Xie, Q. Preparation and optimization of diatom-based cadmium ion-imprinted materials. *J. Mol. Struct.* **2022**, *1251*, 132044. [CrossRef]
17. Awan, M.A.; Qazi, I.A.; Khalid, I. Removal of heavy metals through adsorption using sand. *J. Environ. Sci.* **2003**, *15*, 413–416.
18. Singh, N.B.; Nagpal, G.; Agrawal, S.; Rachna. Water purification by using Adsorbents: A Review. *Environ. Technol. Innov.* **2018**, *11*, 187–240. [CrossRef]
19. Shen, T.-M.; Xu, H.; Miao, Y.; Ma, L.-L.; Chen, N.-C.; Xie, Q.-L. Study on the adsorption process of Cd(II) by Mn-diatomite modified adsorbent. *Mater. Lett.* **2021**, *300*, 130087. [CrossRef]
20. Lo, S.-F.; Wang, S.-Y.; Tsai, M.-J.; Lin, L.-D. Adsorption capacity and removal efficiency of heavy metal ions by Moso and Ma bamboo activated carbons. *Chem. Eng. Res. Des.* **2012**, *90*, 1397–1406. [CrossRef]
21. Li, Y.; Zhu, Y.; Zhu, Z.; Zhang, X.; Wang, D.; Xie, L. Fixed-Bed Column Adsorption of Arsenic(V) by Porous Composite of Magnetite/Hematite/Carbon with Eucalyptus Wood Microstructure. *J. Environ. Eng. Landsc. Manag.* **2018**, *26*, 38–56. [CrossRef]

22. Meng, M.; Meng, X.; Liu, Y.; Liu, Z.; Han, J.; Wang, Y.; Luo, M.; Chen, R.; Ni, L.; Yan, Y. An ion-imprinted functionalized SBA-15 adsorbent synthesized by surface imprinting technique via reversible addition–fragmentation chain transfer polymerization for selective removal of Ce(III) from aqueous solution. *J. Hazard. Mater.* **2014**, *278*, 134–143. [CrossRef]
23. Fu, J.; Wang, X.; Li, J.; Ding, Y.; Chen, L. Synthesis of multi-ion imprinted polymers based on dithizone chelation for simultaneous removal of Hg2+, Cd2+, Ni2+ and Cu2+ from aqueous solutions. *RSC Adv.* **2016**, *6*, 44087–44095. [CrossRef]
24. Wang, Z.; Zhou, C.; Wu, S.; Sun, C. Ion-Imprinted Polymer Modified with Carbon Quantum Dots as a Highly Sensitive Copper(II) Ion Probe. *Polymers* **2021**, *13*, 1376. [CrossRef]
25. Liu, M.; Chen, C.; Wen, T.; Wang, X. Synthesis of magnetic ion-imprinted composites and selective separation and preconcentration of U(VI). *Dalton Trans.* **2014**, *43*, 7050–7056. [CrossRef] [PubMed]
26. Jiang, C.; Fang, M.; Huang, A.; Han, S.; Jin, G.-P. Fabrication of a novel magnetic rubidium ion-imprinted polymer for selective separation. *New J. Chem.* **2022**, *46*, 6343–6352. [CrossRef]
27. Huang, W.; Liu, Y.; Wang, N.; Song, G.; Yin, X.; Zhang, L.; Ni, X.; Xu, W. A Sensitive Electrochemical Sensor Based on Ion Imprinted Polymers with Gold Nanoparticles for High Selective Detecting Cd (II) Ions in Real Samples. *J. Inorg. Organomet. Polym. Mater.* **2021**, *31*, 2043–2053. [CrossRef]
28. Pan, W.; Chen, L.; Wang, Y.; Yan, Y. Selective separation of low concentration rare earths via coordination-induced ion imprinted electrospun membranes. *J. Membr. Sci.* **2022**, *658*, 120759. [CrossRef]
29. Shi, J.; Liu, W.; Yang, S.; Wu, Z.; Han, B.; Li, D.; Xu, X. Adsorption Thermodynamic and Kinetic Mechanism of Substrate-Induced Molecular Geometry Orientation. *Langmuir* **2022**, *38*, 495–503. [CrossRef]
30. Liao, W.; Zhang, X.; Ke, S.; Shao, J.; Yang, H.; Zhang, S.; Chen, H. Effect of different biomass species and pyrolysis temperatures on heavy metal adsorption, stability and economy of biochar. *Ind. Crops Prod.* **2022**, *186*, 115238. [CrossRef]
31. Wu, Y.; Lin, R.; Zhang, K.; Yan, J.; Ma, F.; Zhen, J.; Pan, J. Discontinuous cooperative imprinting idea based on MXene-nanocomposite membrane for high structurally stable recognition and separation of shikimic acid. *Chem. Eng. J.* **2023**, *460*, 141891. [CrossRef]
32. Zhou, G.; Yu, P.; Shen, Y.; Wang, C.; Li, Y.; Yang, R.; Fu, X.; Chi, J.; Chen, X.; Feng, Y. Ion imprinted polymer layer modified magnetic nanocomposites for selective recycling of aqueous Ni(II). *J. Clean. Prod.* **2022**, *373*, 133748. [CrossRef]
33. He, Y.; Wu, P.; Xiao, W.; Li, G.; Yi, J.; He, Y.; Chen, C.; Ding, P.; Duan, Y. Efficient removal of Pb(II) from aqueous solution by a novel ion imprinted magnetic biosorbent: Adsorption kinetics and mechanisms. *PLoS ONE* **2019**, *14*, e0213377. [CrossRef] [PubMed]
34. Liu, F.; Liu, Y.; Xu, Y.; Ni, L.; Meng, X.; Hu, Z.; Zhong, G.; Meng, M.; Wang, Y.; Han, J. Efficient static and dynamic removal of Sr(II) from aqueous solution using chitosan ion-imprinted polymer functionalized with dithiocarbamate. *J. Environ. Chem. Eng.* **2015**, *3*, 1061–1071. [CrossRef]
35. He, G.; Li, Z.; Liu, Y.; Liu, M.; Zhu, C.; Zhang, L.; Zhang, H. A novel lithium ion-imprinted membrane with robust adsorption capacity and anti-fouling property based on the uniform multilayered interlayer. *Desalination* **2022**, *539*, 115973. [CrossRef]
36. Ali, I.M.; Zakaria, E.S.; Khalil, M.; El-Tantawy, A.; El-Saied, F.A. Synthesis of ion-imprinted polymers based on chitosan for high selectivity of La(III), Ce(III) and Sm(III) via solid phase extraction. *J. Mol. Liq.* **2022**, *356*, 119058. [CrossRef]
37. Liu, Y.; Qiu, J.; Jiang, Y.; Liu, Z.; Meng, M.; Ni, L.; Qin, C.; Peng, J. Selective Ce(III) ion-imprinted polymer grafted on Fe3O4 nanoparticles supported by SBA-15 mesopores microreactor via surface-initiated RAFT polymerization. *Microporous Mesoporous Mater.* **2016**, *234*, 176–185. [CrossRef]
38. Liu, Y.-X.; Bian, L.-C.; Xia, J.-R.; Cao, Q.-E. A Novel Ion-imprinted Polymer Based on Multi-walled Carbon Nanotubes for Solid Phase Extraction of Pd(II). *Chin. J. Anal. Chem.* **2021**, *49*, e21170–e21178. [CrossRef]
39. Fei, J.J.; Wu, X.H.; Sun, Y.L.; Zhao, L.Y.; Min, H.; Cui, X.B.; Chen, Y.J.; Liu, S.; Lian, H.Z.; Li, C. Preparation of a novel amino functionalized ion-imprinted hybrid monolithic column for the selective extraction of trace copper followed by ICP-MS detection. *Anal. Chim. Acta* **2021**, *1162*, 338477. [CrossRef]
40. Xu, X.; Wang, M.; Wu, Q.; Xu, Z.; Tian, X. Synthesis and Application of Novel Magnetic Ion-Imprinted Polymers for Selective Solid Phase Extraction of Cadmium (II). *Polymers* **2017**, *9*, 360. [CrossRef] [PubMed]
41. Wu, X.; Wang, X.; Hu, Y.; Chen, H.; Liu, X.; Dang, X. Adsorption mechanism study of multinuclear metal coordination cluster Zn5 for anionic dyes congo red and methyl orange: Experiment and molecular simulation. *Appl. Surf. Sci.* **2022**, *586*, 152745. [CrossRef]
42. Zhao, Z.; Zhang, X.; Ruan, D.; Xu, H.; Wang, F.; Lei, W.; Xia, M. Efficient removal of heavy metal ions by diethylenetriaminepenta (methylene phosphonic) acid-doped hydroxyapatite. *Sci. Total Environ.* **2022**, *849*, 157557. [CrossRef] [PubMed]